University of Leipzig

Advanced Labs

Lab report

Rotation-Vibration Spectra of Molecules

Jamal Ghaith 3792970

Anas Roumieh 3766647

Conducted on:

Contents

1 Introduction **1**
1.1 FTIR Spectroscopy . . . 1
1.2 Rotation-Vibration Spectra of diatomic molecules . . . 2
1.3 Interference Method . . . 5
1.4 Intensity of rotational-vibrational spectra . . . 6
1.5 Experimental Setup . . . 7

2 Analysis **8**
2.1 Task 1 . . . 8
2.2 Task 2 . . . 9
2.2.1 Calibration . . . 9
2.2.2 Zerofilling . . . 10
2.2.3 Apodization . . . 11
2.2.4 Comparison . . . 11
2.2.5 Step Size and Theoretical Spectral Resolution . . . 12
2.3 Task 3 . . . 13
2.4 Task 4 . . . 14
2.5 Task 5 . . . 14
2.6 Task 6 . . . 17

3 Conclusion **18**

Appendices **19**

A Task 1 **19**
A.1 Plots . . . 19
A.2 Tables . . . 19

B Task 2 **20**

Bibliography **21**

1 Introduction

1.1 FTIR Spectroscopy

FTIR spectroscopy is used to investigate various physical properties of substances or to identify unknown substances through their characteristic spectra. The Spectrum 100 spectrometer operates on the principle of a Michelson interferometer.

A blackbody radiator is used in the spectrometer, emitting a beam of light that strikes a semi-transparent mirror functioning as a beam splitter. The first partial beam follows a fixed path, being reflected by a mirror, then passing through the sample before reaching the detector. However, interference with the second partial beam, which is reflected by a moving mirror and therefore has a variable path difference compared to the first partial beam, occurs prior to the sample. The spectrometer records the intensity of the transmitted light as a function of the mirror apparatus's travel distance. This recording is called an interferogram, which must be transformed into a spectrum via Fourier transformation. FTIR spectrometers show high wavenumber accuracy, typically within a few cm^{-1}.

To enhance the quality of the spectrum display, several methods are employed:

1. **Apodization**: Apodization smooths the abrupt truncation of the interferogram by multiplying it with an apodization function, resulting in a gradual decline. This reduces spectral disturbances, known as the leakage effect. Depending on the function used for multiplication, the decline may be more or less steep. However, a stronger apodization function results in lower spectral resolution.
2. **Zerofilling**: Zerofilling involves supplementing the measured data with additional zeros, resulting in more data points, increasing the quality of the plot. It also mitigates the picket fence effect, where transmission minima may be less discernible or entirely missed due to excessive spacing between data points. However, it is important to note that zerofilling does not enhance the actual information content of the measurement; it merely increases the number of points displayed in the spectrum.
3. **Phase Correction**: Initially, the Fourier transformation converts the unidirectional interferogram into a complex spectrum. Phase correction is then applied to convert this complex spectrum back into a real spectrum.

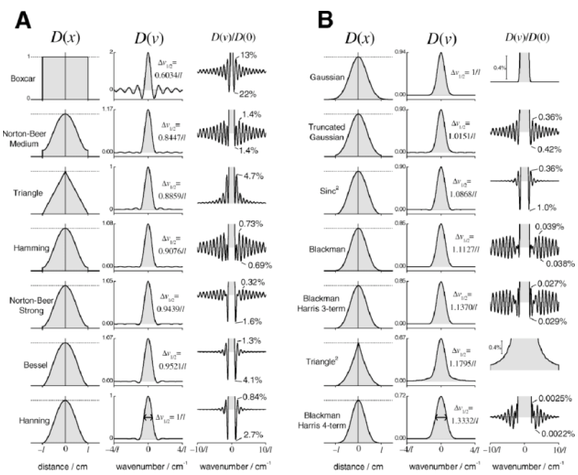

Figure 1: Various Apodization functions and their Fourier Transforms. [1]

Once the spectrum has been generated, it must be divided by a reference spectrum to obtain accurate measurement values for the sample.

1.2 Rotation-Vibration Spectra of diatomic molecules

In diatomic molecules, there is a along the axis connecting the two atoms. Absorption in the infrared range is caused by the various rotations and vibrations of the molecules, which alter the electric dipole moment. In a highly simplified model, the molecule can be represented by a dumbbell, where the masses of the atoms are treated as point masses that rotate at a fixed distance around a fixed axis through the center of gravity.

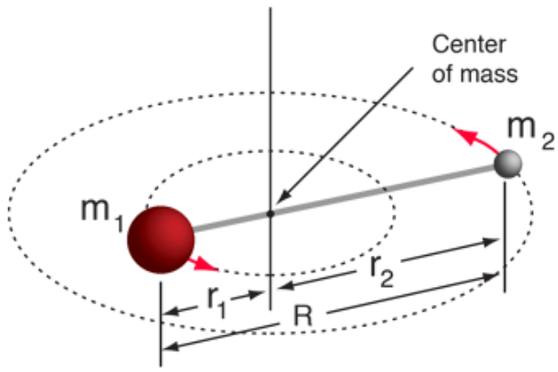

Figure 2: Dumbbell model of a diatomic molecule. [3]

The moment of inertia of the dumbbell is given by

$$I = \mu r^2,$$

where the reduced mass μ is

$$\mu = \frac{m_1 m_2}{m_1 + m_2}.$$

Solving the Schrödinger equation in polar coordinates with a vanishing potential yields discrete energy values:

$$E_m = \frac{m^2 h^2}{8\pi^2 \mu r^2}.$$

Next, this dumbbell model can be considered in the context of rotation around a space-free axis, so we transition to spherical coordinates. In this scenario, the energy is given by

$$E(J) = hcBJ(J+1) \quad \text{for} \quad J \in \mathbb{N}_0,$$

with the rotation constant

$$B = \frac{h}{8\pi^2 cI}.$$

The rotational term thus becomes

$$F(J) = \frac{E}{hc} = BJ(J+1) \quad \text{for} \quad J \in \mathbb{N}_0,$$

subject to the selection rule

$$\Delta J = \pm 1.$$

In addition, the harmonic oscillator can be considered, initially in isolation.

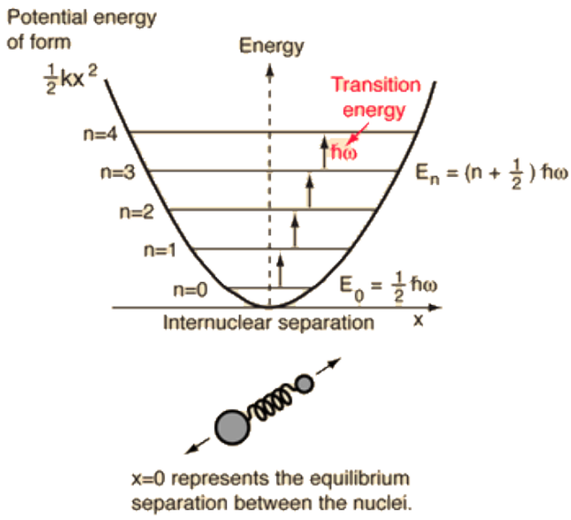

Figure 3: Harmonic Oscillator model of a diatomic molecule. [2]

Here, the equations of motion are obtained by considering the forces:

$$m_1\ddot{x}_1 = -k(x_1 - x_2),$$
$$m_2\ddot{x}_2 = -k(x_2 - x_1).$$

By introducing the substitution $x = x_1 - x_2$, these equations can be combined into:

$$\ddot{x} = -\frac{k}{\mu}x,$$

where the reduced mass μ is defined as:

$$\mu = \frac{m_1 m_2}{m_1 + m_2}.$$

The resonance wavenumber of such a harmonic oscillator is then given by:

$$\bar{\nu}_s = \frac{1}{2\pi c}\sqrt{\frac{k}{\mu}}.$$

To calculate the energy values, we solve the Schrödinger equation for the potential:

$$U = 2\pi^2 c^2 \bar{\nu}_s^2 \mu x^2,$$

which is derived from the restoring force:

$$-\frac{dU}{dx} = F = -kx.$$

Assuming a solution of the form:

$$x = x_0 \sin(2\pi c\bar{\nu}_s t),$$

we obtain discrete energy levels:

$$E(n) = hc\bar{\nu}\left(n + \frac{1}{2}\right), \quad n \in \mathbb{N}_0,$$

with the selection rule:

$$\Delta n = \pm 1.$$

These energy levels in turn yield the oscillation term:

$$G(n) = \bar{\nu}_s \left(n + \frac{1}{2} \right).$$

Both effects can now be combined to obtain the rotational-vibrational spectra. If interactions are initially neglected, the rotational and vibrational energy can be summed up as:

$$E(n, J) = hcBJ(J+1) + hc\bar{\nu}_s \left(n + \frac{1}{2} \right),$$

resulting in the rotational oscillation term:

$$T(n, J) = BJ(J+1) + \bar{\nu}_s \left(n + \frac{1}{2} \right).$$

Transitions are allowed for:

$$\Delta J = \pm 1 \quad \text{and} \quad \Delta n = 0, \pm 1.$$

The transitions can be categorized into the R branch, where J increases, and the P branch, where J decreases. A pure rotational spectrum is obtained for transitions with $n = \text{const}$. To account for the interactions between oscillation and rotation, one must transition from the dumbbell model to the non-rigid rotator model, resulting in the oscillation term as a function of the quantum number:

$$F_n(J) = B_n J(J+1) - D_n J^2 (J+1)^2,$$

where D_n is the respective strain constant. The n-dependence arises from changes in the mean distance between the atoms. If each transition is indexed by i (where $i = \Delta J$), a relationship between the respective wavenumber of the minimum and the quantum number-dependent rotation and strain constants can be expressed as:

$$\bar{\nu}_i = \bar{\nu}_s + (B_1 + B_0)i + (B_1 - B_0)i^2 - 2(D_1 + D_0)i^3 \tag{1}$$

If we calculate the difference between two neighboring wavenumber minima and then the difference between these differences, we obtain the following equations:

$$\Delta\bar{\nu}(i) = 2B_1 - 2(D_1 + D_0) + 2i(B_1 - B_0 - 3(D_1 + D_0)) - 6i^2(D_1 + D_0), \tag{2}$$

If a quadratic fit is performed on 2, one can figure out the values of $D_1 + D_0$, B_1 and B_0.

1.3 Interference Method

When a light beam passes through an empty cuvette, multiple reflections occur, leading to interference. These interferences depend on the wavelength of the light, the thickness and refractive index of the cavity, and the angle of incidence. In the spectrum, they manifest as a periodic modulation of the intensity. The following sections outline the theoretical principles that describe the wavelengths corresponding to the transmission maxima and minima.

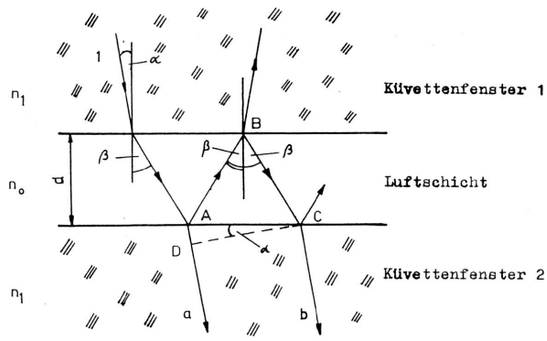

Figure 4: Interference in a thin film. The labels from top to bottom are cuvette window 1, air gap, cuvette window 2. [4]

Whether this interference is constructive or destructive depends on the path difference between the waves. This path difference is given by:

$$\Delta = n_0(\mathrm{AB} + \mathrm{BC}) - n_1 \mathrm{AD},$$

and can be calculated using trigonometric relationships and Snell's law of refraction:

$$n_0 \sin\beta = n_1 \sin\alpha,$$

which leads to:

$$\Delta = 2n_0 d \cos\beta.$$

Destructive interference occurs when the path difference is a half-integer multiple of the wavelength, and constructive interference occurs for integer multiples. The difference between the ordinal numbers of the maxima is given by:

$$N_1 - N_2 = 2dn_0(\bar{\nu}_1 - \bar{\nu}_2),$$

which results in the film thickness for an air-filled cell ($n_0 \approx 1$) being

$$d = \frac{N_1 - N_2}{2(\bar{\nu}_1 - \bar{\nu}_2)}. \tag{3}$$

1.4 Intensity of rotational-vibrational spectra

Consider the number of molecules N in the state with $n = 0$. The expression for $N(J, n = 0)$ is given by:

$$N(J, n = 0) = \frac{N_{\text{gas}}}{Q_r}(2J + 1) \exp\left(-\frac{hcBJ(J + 1)}{kT}\right) \exp\left(-\frac{hc\bar{\nu}_s(n + \frac{1}{2})}{kT}\right)$$

where Q_r represents the sum of the states.

For the absorption coefficient, which is critical for determining the intensity of the minima, we have:

$$\alpha = c_3\bar{\nu}(2J + 1) \exp\left(-\frac{hcBJ(J + 1)}{kT}\right)$$

where c_3 is a constant. According to Lambert-Beer's law, the relative intensities are:

$$I(J) = I_0 \exp(-\alpha d) = I_0 \exp\left(-c_4\bar{\nu}(2J + 1) \exp\left(-\frac{hcBJ(J + 1)}{kT}\right)\right) \tag{4}$$

where $\bar{\nu}$ is found using 1

1.5 Experimental Setup

We used the Perkin Elmer Spectrum 100 FTIR spectrometer. This instrument operates using a modified Michelson interferometer. In this configuration, the path difference between the two light beams is adjusted by rotating an additional pair of mirrors around a common axis.

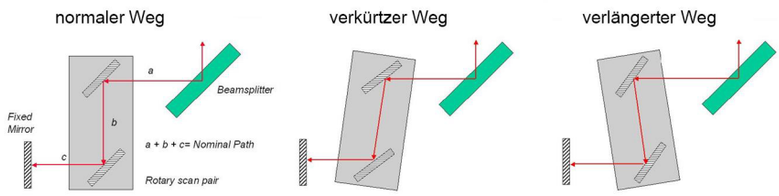

Figure 5: Path difference via a rotatable mirror apparatus. [4]

The light source for the spectrometer is a 'Norton Source' which is a silicon carbide crystal through which a current flows. The current heats the crystal, causing it to emit an almost perfect blackbody spectrum with its peak in the mid-infrared range.

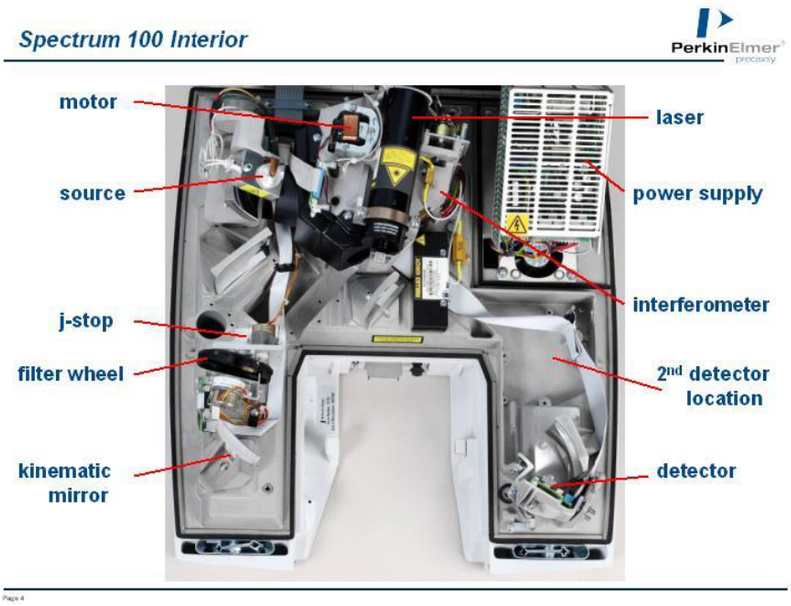

Figure 6: Structure inside the Spectrum 100 spectrometer. [4]

For the measurement, the sample is placed in the cuvette holder of the spectrometer. Once the lid is closed and the measurement is initiated, the spectrometer records an interferogram. The travel distance of the mirror apparatus can be adjusted according to the requirements of the measurement. Depending on the selected measurement mode, the spectrum can either be directly generated by the device or calculated manually using a Fourier transform.

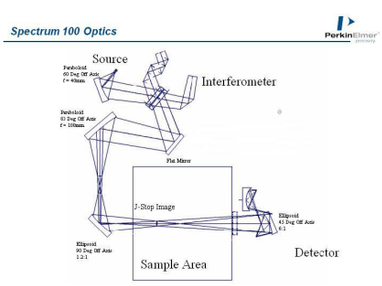

(a) Schematic of the optics inside the spectrometer. [4]

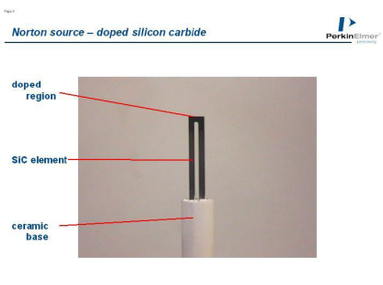

(b) Norton Source.

Figure 7

2 Analysis

2.1 Task 1

Verify the calibration of the wavenumber scale of the infrared spectrometer Spectrum 100 using water vapor and polystyrene calibration bands. Plot the experimentally determined deviations and discuss them.

When measuring the spectrum of "water vapour", what we are actually measuring is the empty cuvette holder with air inside it, as a background spectrum that will prove useful later. The following plots show the spectra for water vapour and polystyrene:

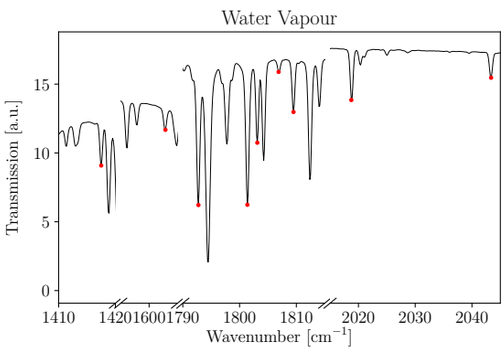

(a) Water Vapour Spectrum, with the dips marked by red dots. Only the useful parts of the graph are shown; with ranges of $\bar{\nu} = 1410 - 1420,\ 1595 - 1605,\ 1790 - 1815,\ 2015 - 2045\,\mathrm{cm}^{-1}$.

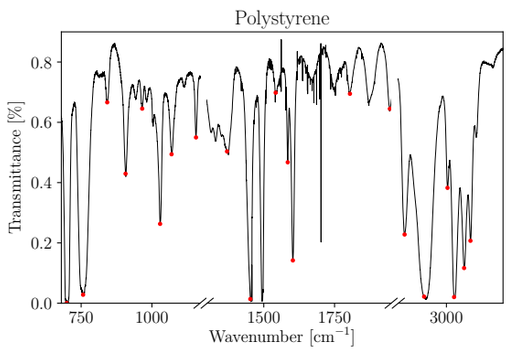

(b) Polystyrene Spectrum, with the dips marked by red dots. Only the useful parts of the graph are shown; with ranges of $\bar{\nu} = 680 - 1170,\ 1300 - 1950,\ 2830 - 3200\,\mathrm{cm}^{-1}$.

Figure 8: Useful parts of the water vapour and polystyrene spectra. Full plots found in Appendix A.1

The tables in Appendix A.2 show the comparison between the experimentally found dip wavenumbers and the ones provided in [4]. The following plot show the deviations from the theoretical values:

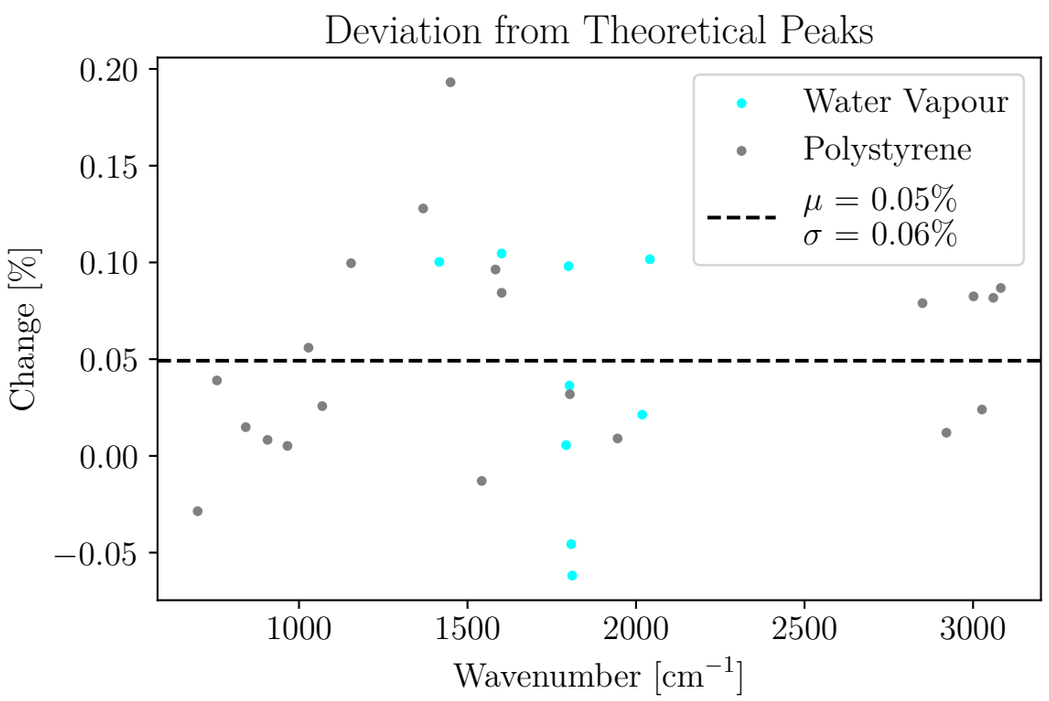

Figure 9: Deviations of the experimentally found wavenumbers from the theoretical ones for both water vapour and polystyrene.

Since the deviations should be device-dependent rather than sample-dependent, they can be plotted together for a better average. The average percentage change was around 0.05% with a standard deviation of 0.06%. In wavenumbers, this amounts to an average of $0.92\mathrm{cm}^{-1}$ and a standard deviation of $1.04\mathrm{cm}^{-1}$ This shows that the device is well-calibrated as the deviations are well-within acceptable an acceptable range.

2.2 Task 2

Acquire interferograms of the water vapor spectrum using different mirror ranges of the interferometer. Obtain the spectra by a applying a Fourier transformation to these interferograms. Calibrate the wavenumber scale of the thereby obtained spectra using the values for the water vapor bands. Determine step size of the optical path from the band width of the spectrum. Discuss the influence of the interferogram length and the applied zerofilling and apodisation on the spectral resolution based on the spectra. Based on the calculated step size, give the theoretical spectral resolution in dependence on the recorded data point count.

2.2.1 Calibration

When converting the raw interferograms to spectra, the x-axis needs to be calibrated. As the raw data has a scale of mirror position, and the fourier transform is just a frequency of those, rather than a wavenumber. The following figure shows the raw and fourier transformed data for the maximum mirror range:

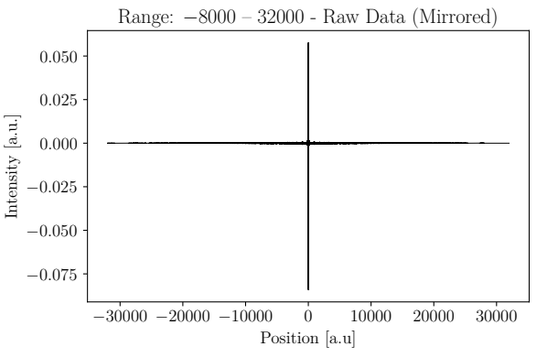

(a) Raw Spectrum.

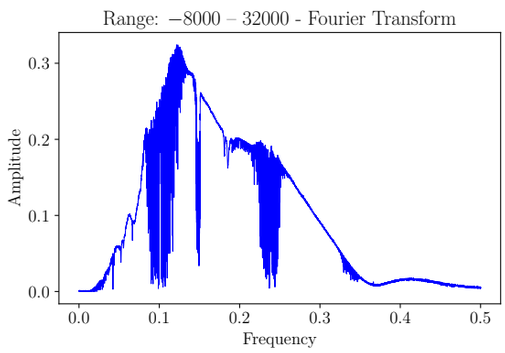

(b) Fourier Transformed Spectrum. No apodisation or zerofilling.

Figure 10: Raw and Fourier Transformed data

To calibrate the wavenumber scale, the wavenumbers of the water vapour bands are used, in a fashion similar to Figure 8a. The following figure shows the calibration of the wavenumber scale for the maximum mirror range:

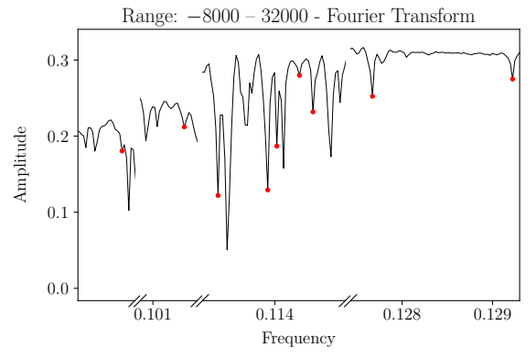

(a) Fourier Transformed spectrum with the dips marked by red dots. Only useful parts of the spectrum are shown.

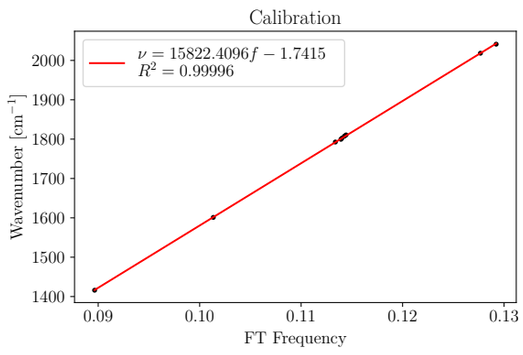

(b) Linear fit between dip 'frequencies' in Figure 11a and calibration bands in [4].

Figure 11: Calibration of the frequency scale

This linear function can now be used to convert from the frequency scale to the wavenumber scale. Since all known dips were used, and we have a high R^2 value, this equation is very reliable.

2.2.2 Zerofilling

Zerofilling is a technique used to increase the quality (but not resolution) of the spectrum by adding zeros to the end of the interferogram before fourier transforming, increasing the number of data points in the spectrum. The following figure shows the effect of zerofilling on a spectrum with a lower resolution:

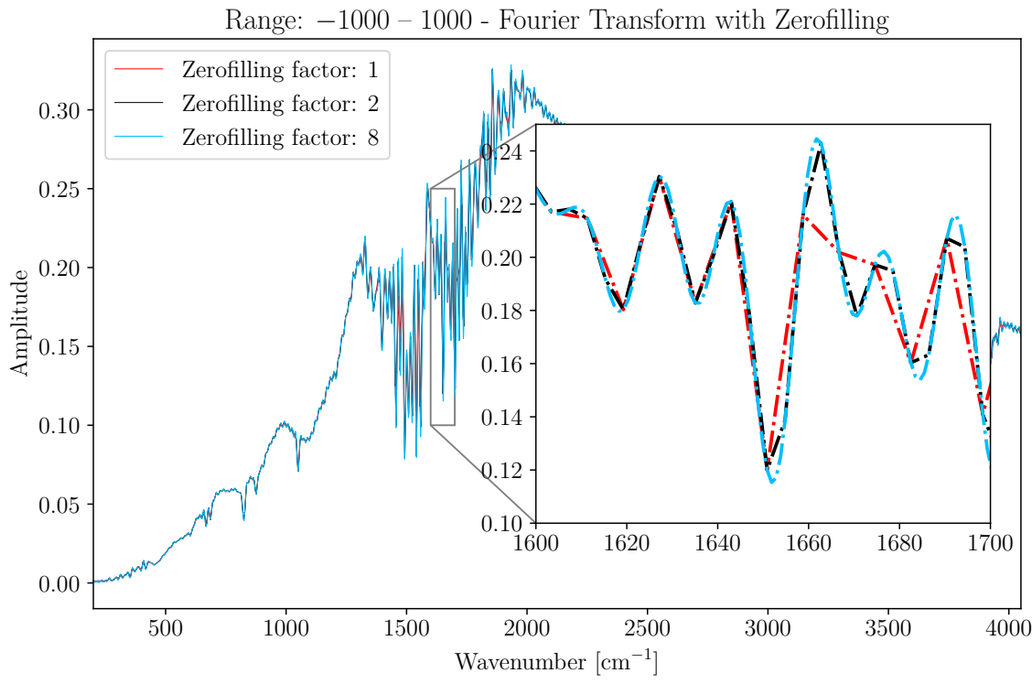

Figure 12: Spe5ctrum with various factors of zerofilling. Inset axes show a zoomed in part of the spectrum where the effect is shown, and lines are dashed for better legibility.

Here the low resolution spectrum benefits from zerofilling, as the minima near 1670 cm^{-1} are more pronounced.

2.2.3 Apodization

Apodization is the process of applying a window function before the fourier transform is performed, reducing the "leakage effect" of a fourier transform. This happens due to the fact that fourier transforms need to be infinite, meaning you require a periodic signal to perform a fourier transform. If the signal is not periodic, there will be jumps in whatever is being transformed which can manifest as small amplitude modulations. A windowing/ apodization function will make the ends of what is being transformed close to zero such that the signal now looks periodic. The following figure shows the effect of apodization on a fourier transform:

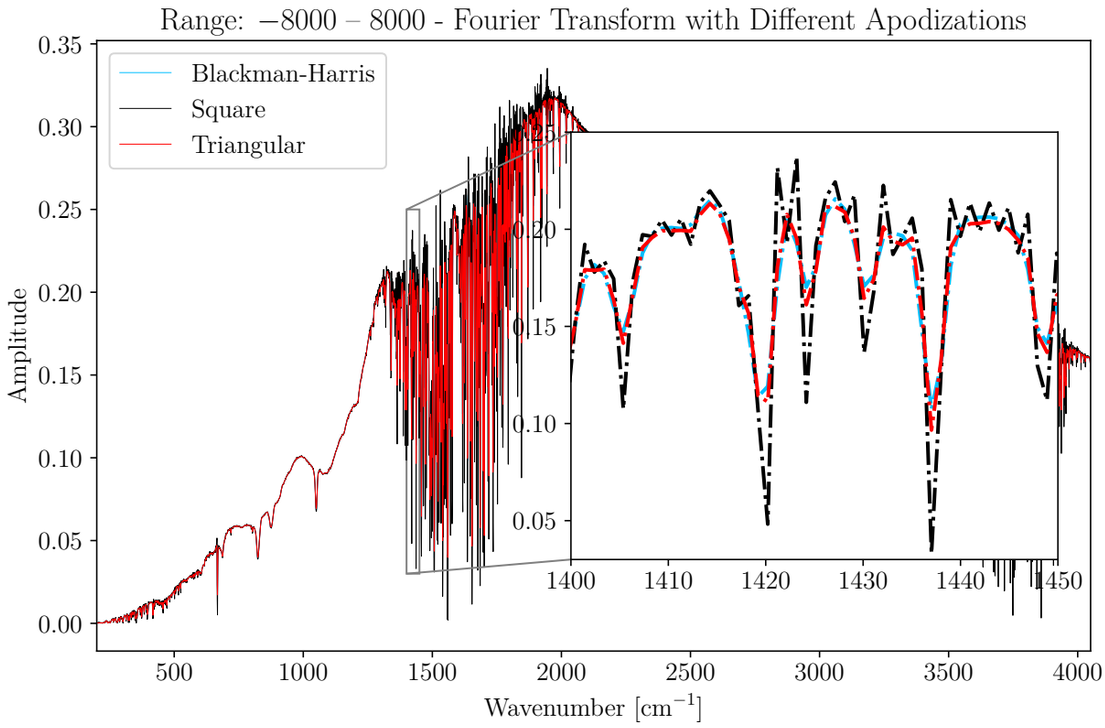

Figure 13: Spectrum with various apodization functions. Inset axes show a zoomed in part of the spectrum where the effect is shown, and lines are dashed for better legibility.

The square apodization function is just the default way an FFT is performed, so it is considered as "no apodization". The 3 Term Blackman-Harris and Triangular apodization functions show a decrease in noise between the dips, but the dips themselves are less pronounced.

2.2.4 Comparison

Here, the difference between the spectrum at the maximum mirror range, with Blackman-Harris apodization and no zerofilling is compared to the spectrum with a lower mirror range, a zero-filling factor of 8 and no apodization. The following figure shows the two plots in the ranges used in Figure 8a:

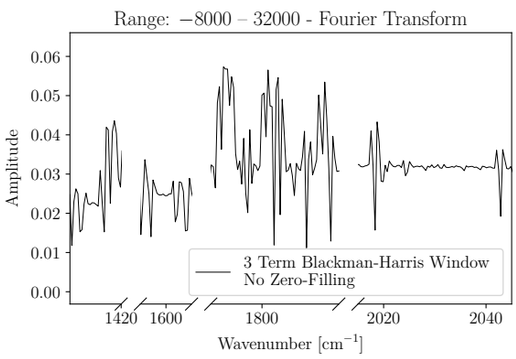

(a) Maximum Mirror Range, no Zerofilling, Blackman-Harris Apodization.

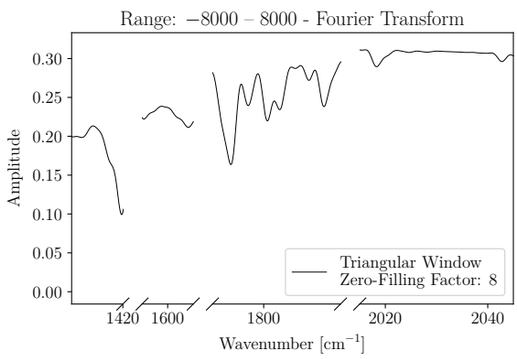

(b) Lower Mirror Range, Zerofilling factor of 8, no Apodization.

Figure 14: Comparison of the two spectra

We chose this range as it is a good benchmark to compare to. Full figures are shown in Appendix B.

Figure 14a shows more pronounced dips compared to Figure 8a, but the noise is also more pronounced. Compared to Figure 14b, it shows more dips but this is only due to the higher resolution of the measurement. 14b shows less pronounced dips (and sometimes no dips due to the lower resolution), but they are much smoother and clearer to identify.

2.2.5 Step Size and Theoretical Spectral Resolution

The spectrometer operates in the mid-infrared range, so the wavelengths are between 2.5μm and 50μm, meaning the maximum wavenumber is $\bar{\nu} = 4000$ cm^{-1}. The step size is therefore

$$\Delta x = \frac{1}{2\bar{\nu}_{\max}} = \frac{1}{2 \cdot 4000} = \boxed{1.25 \cdot 10^{-4} \text{ cm}}$$

So the theoretical spectral resolution given a number of measuring points n is

$$\Delta\nu = \frac{1}{n\Delta x} = \boxed{\frac{8000}{n} \text{ cm}^{-1}}$$

2.3 Task 3

Determine the detected signal strength in the blocking range of a glass and a NaCl blocking filter.

The following figure shows the spectra of the glass and NaCl blocking filters:

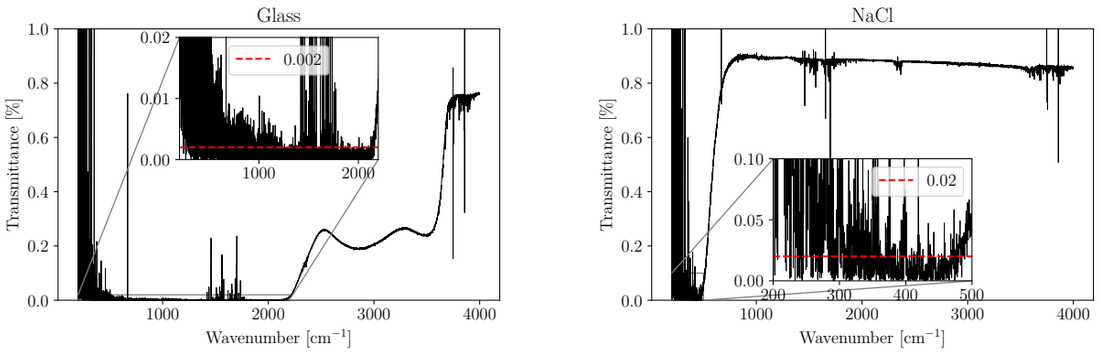

(a) Glass Blocking Filter.

(b) NaCl Blocking Filter.

Figure 15: Spectra of the glass and NaCl blocking filters. Inset axes show a zoomed in part of the spectrum where the filter blocks the signal

It is clear that Glass blocks wavenumbers below $\approx$ 2100 cm^{-1}, while NaCl blocks wavenumbers below $\approx$ 500 cm^{-1}. However, the signal strength is not zero there, as the filters are not perfect. Moreover, our data for water vapour in Task 2 is oddly noisey in the lower wavenumbers, so the signal strength is not as clear as it should be.

It is still somewhat reasonable to assume that glass blocks the signal 10 times better than the NaCl filter, as seen by their signal strengths.

Further adding to the noise problem is that both spectra can have low values near low wavenumbers, and since we are normalizing with respect to the water vapour spectrum, small fluctations cause large changes.

2.4 Task 4

In this task, the gap width of a cuvette was determined using the interference method. From Fig. 16a, 10 points of interference dips were extracted and plotted against over the corresponding wavelength. Linear regression was performed on the data points to determine the slope of the line which is twice the gap width of the cuvette. Eq. 3 was used. The gap width was found to be $d = 47.52 \pm 0.15$ μm.

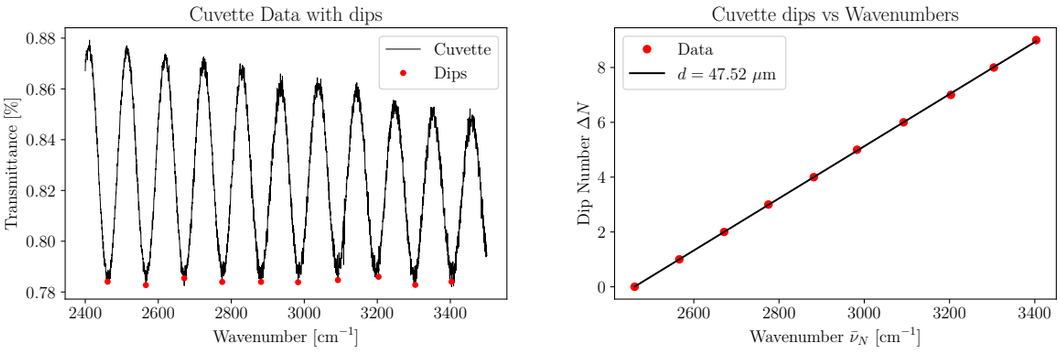

(a) Cuvette dips

(b) Cuvette fit

2.5 Task 5

This task analyzes the rotation-vibration spectrum of HCl. The data in this task was provided by our supervisor. The relevant part of the spectrum (after considering the background effects) is shown in Fig. 17. The dips corresponding to absorption of the two Chlorine isotopes ^{35}Cl and ^{37}Cl were identified. The left dip corresponds to ^{37}Cl and the right dip corresponds to ^{35}Cl.

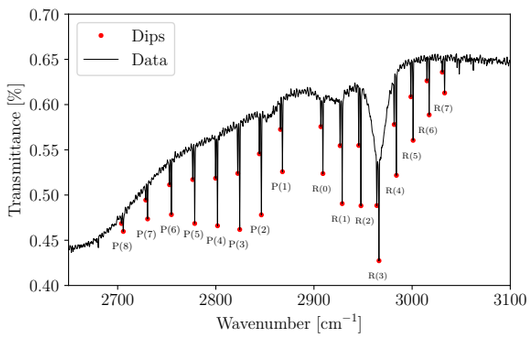

Figure 17: HCl spectrum

We can clearly see the R- and P-branches in the spectrum. The R-branch is the one with the higher wavenumbers, while the P-branch is the one with the lower wavenumbers. The wavenumbers of the R- and P-branches were determined. The results are shown in Tables 1 & 2. The gap between the two branches is due to $\Delta J = -1$ in the P-branch. The symbol $P(J)$ means an initial state with J with $\Delta J = -1$ as the transition happens. Hence, we see that the P-branch must start at $J = 1$.

Minimum	Index i	$\bar{\nu}\left(^{35}\text{Cl}\right)$ [cm^{-1}]	$\bar{\nu}\left(^{37}\text{Cl}\right)$ [cm^{-1}]
P(8)	-8	2705.75	2703.875
P(7)	-7	2730.5	2728.625
P(6)	-6	2754.75	2752.875
P(5)	-5	2778.5	2776.5
P(4)	-4	2801.75	2799.75
P(3)	-3	2824.375	2822.375
P(2)	-2	2846.375	2844.375
P(1)	-1	2867.875	2865.875

Table 1: P-branch wavenumbers

Minimum	Index i	$\bar{\nu}\left(^{35}\mathrm{Cl}\right)\ [\mathrm{cm}^{-1}]$	$\bar{\nu}\left(^{37}\mathrm{Cl}\right)\ [\mathrm{cm}^{-1}]$
R(0)	1	2909.125	2907
R(1)	2	2928.75	2926.625
R(2)	3	2947.875	2945.625
R(3)	4	2966.25	2964
R(4)	5	2984	2981.75
R(5)	6	3001	2998.75
R(6)	7	3017.375	3015.125
R(7)	8	3033.125	3030.75

Table 2: R-branch wavenumbers

The data can be used to find the wavenumber of the purely vibrational transition ν_s, the force constant k, the rotation constant B, the distance of the two atoms in the molecule r_0 and the moment of inertia I. The results are shown in Table 3. The following equations were used:

$$\nu_s = \frac{\nu_R(0) + \nu_P(1)}{2} \tag{5}$$

$$B = \frac{\nu_R(1) - \nu_P(1)}{4} \tag{6}$$

Parameter	^{35}Cl	^{37}Cl
$\bar{\nu}_s\ [\mathrm{cm}^{-1}]$	2888.50 ± 1.37	2886.44 ± 1.37
$B\ [\mathrm{cm}^{-1}]$	10.31 ± 0.69	10.28 ± 0.69
$\mu[\mathrm{u}]$	0.9796	0.9811
$k\ [\mathrm{Nm}^{-1}]$	481.55 ± 0.46	481.60 ± 0.46
$I\ [\mathrm{kgm}^2]$	$2.71 \cdot 10^{-47} \pm 1.82 \cdot 10^{-48}$	$2.72 \cdot 10^{-47} \pm 1.83 \cdot 10^{-48}$
$r_0[\mathrm{m}]$	$1.29 \cdot 10^{-10} \pm 6.12 \cdot 10^{-12}$	$1.29 \cdot 10^{-10} \pm 6.15 \cdot 10^{-12}$

Table 3: Parameters for isotopes of Chlorine

To determine the parameters B_0 , B_1 and D, the first order difference of the wavenumbers is plotted for the two isotopes (we used $D \approx D_0 \approx D_1$) against the peak indicies. A quadratic curve fit was performed using Eq. 2 for each isotope.

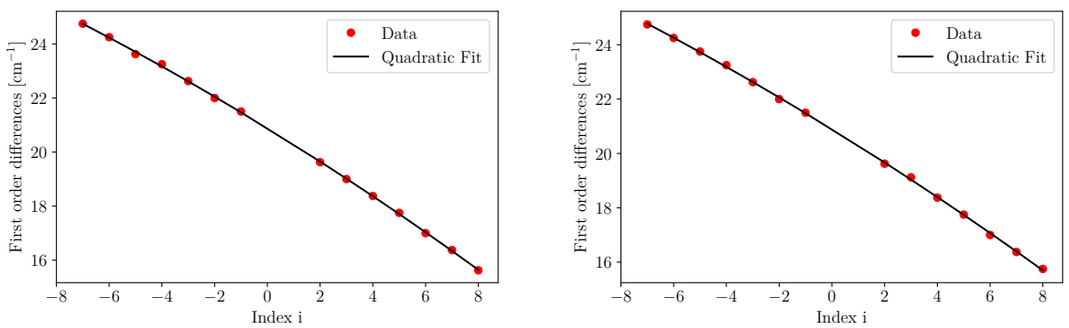

(a) ^{35}Cl (b) ^{37}Cl

Figure 18: Quadratic fits for isotopes of Chlorine

The resulting parameters are shown in Table 4.

Parameter	^{35}Cl	^{37}Cl
$B_0\ [\mathrm{cm}^{-1}]$	10.143 ± 0.012	10.135 ± 0.011
$B_1\ [\mathrm{cm}^{-1}]$	10.445 ± 0.011	10.439 ± 0.011
$D\ [\mathrm{cm}^{-1}]$	$0.00052 \pm 6.09 \times 10^{-5}$	$0.00056 \pm 5.47 \times 10^{-5}$

Table 4: Parameters for ^{35}Cl and ^{37}Cl

The spectral splitting is found to be:

Index	Value
−8	2.375
−7	2.25
−6	2.25
−5	2.25
−4	2.25
−3	2.25
−2	2.125
−1	2.125
1	2.0
2	2.0
3	2.0
4	2.0
5	2.0
6	1.875
7	1.875
8	1.875

Table 5: Values of the splitting between the two isotopes

To find the ratio between the two isotopes, we had to adjust the spectrum to eliminate other sources of absorption. The minima were masked and the remaining data was interpolated using the cubic spline method. The interpolated data was then renormalized using this cubic spline to obtain the intensity. This process is shown in Fig. 19.

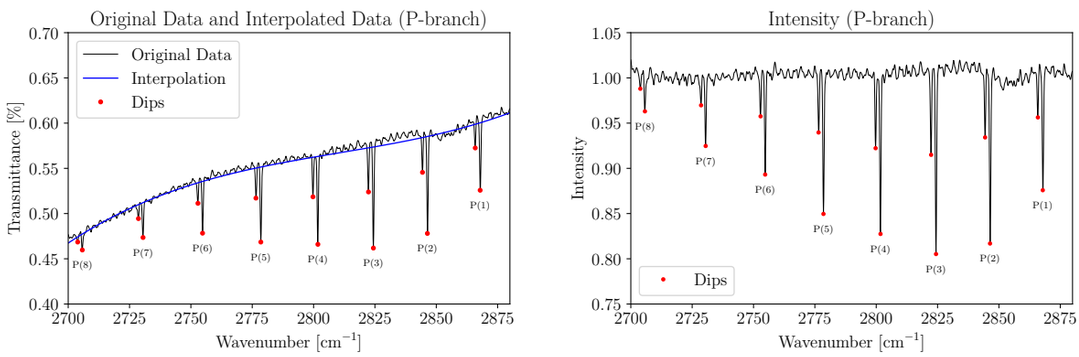

Figure 19: Interpolating the data

Using Lambert-Beer's law 4, we find out that ^{35}Cl makes up about 68% of the atoms with the remaining 32% being ^{37}Cl, since these are the only stable isotopes, which is a decent approximation to the actual value of 75%.

2.6 Task 6

Using the same interpolated data, the intensities of the minima was plotted against the rotational quantum number J. A curve fit was carried out using Lambert-Beer's law 4 for each isotope. The results are shown in Fig. 20.

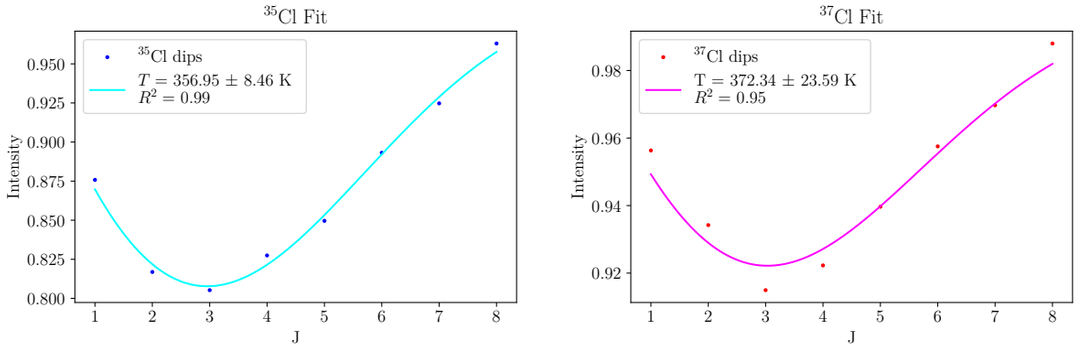

(a) ^{35}Cl (b) ^{37}Cl

Figure 20: Fitting the intensities to determine the temperature

The temperatures obtained from the fits are:

$$T_{^{35}\mathrm{Cl}} = 356.95 \pm 8.46 \text{ K}$$
$$T_{^{37}\mathrm{Cl}} = 372.34 \pm 23.59 \text{ K}$$

Which is 20% and 25% off from room temperature of 293.15 K for ^{35}Cl and ^{37}Cl, respectively.

This error is unexpectedly high, and could be due to the difficulty of fitting the data, which took some effort to get right. Also, the interpolation method used also probably introduced some error.

3 Conclusion

In this report, we have verified the calibration of the wavenumber scale of the infrared spectrometer Spectrum 100 using the spectra of water vapor and polystyrene. The deviations from the theoretical wavenumbers were minimal, with an average deviation of 0.92 cm^{-1} and a standard deviation of 1.04 cm^{-1}, confirming that the device is well-calibrated.

We explored the impact of mirror range, zerofilling, and apodization on the spectral resolution and noise levels. The calibration of the wavenumber scale was successfully achieved by correlating the known wavenumbers of water vapor bands with the frequencies obtained from the Fourier transform of the interferograms. The effect of zerofilling was observed to enhance the appearance of spectral features without improving resolution, while apodization reduced noise but slightly diminished the prominence of spectral dips.

In the examination of the blocking filters, it was evident that glass and NaCl filters effectively block certain ranges of wavenumbers, though some signal leakage was observed, particularly at lower wavenumbers. The glass filter exhibited stronger blocking capabilities compared to the NaCl filter.

The analysis of the rotation-vibration spectrum of HCl allowed us to identify the isotopic contributions of ^{35}Cl and ^{37}Cl, and calculate key molecular parameters such as the vibrational transition wavenumber (ν_s), rotational constant (B), bond length (r_0), and force constant (k). The results were consistent with theoretical expectations, confirming the accuracy of the measurements.

Appendices

A Task 1

A.1 Plots

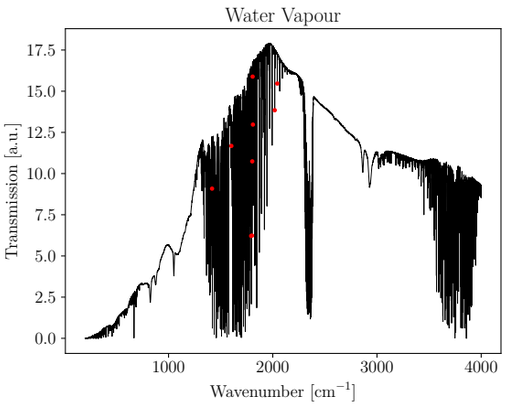

(a) Full Water Vapour Spectrum. Dips are marked by red dots.

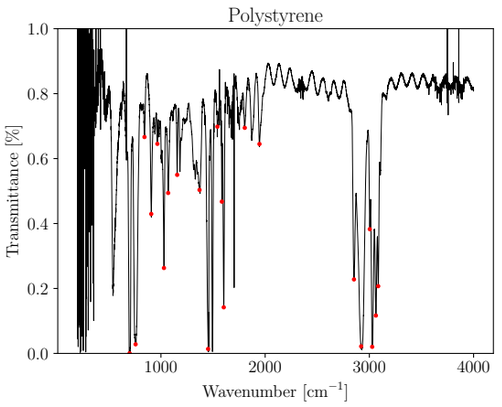

(b) Full Polystyrene Spectrum. Dips are marked by red dots.

Figure 21

A.2 Tables

Polystyrene			
Theoretical [cm^{-1}]	Experimental [cm^{-1}]	$\Delta\bar{\nu}$ [cm^{-1}]	% Error
699.450	699.250	-0.200	-0.029
756.580	756.875	0.295	0.039
842.000	842.125	0.125	0.015
906.800	906.875	0.075	0.008
965.700	965.750	0.050	0.005
1028.300	1028.875	0.575	0.056
1069.100	1069.375	0.275	0.026
1154.600	1155.750	1.150	0.100
1449.700	1452.500	2.800	0.193
1368.500	1370.250	1.750	0.128
1542.200	1542.000	-0.200	-0.013
1583.100	1584.625	1.525	0.096
1601.400	1602.750	1.350	0.084
1803.800	1804.375	0.575	0.032
1945.200	1945.375	0.175	0.009
2850.000	2852.250	2.250	0.079
2920.900	2921.250	0.350	0.012
3001.400	3003.875	2.475	0.082
3026.400	3027.125	0.725	0.024
3060.000	3062.500	2.500	0.082
3082.200	3084.875	2.675	0.087

Table 6

Water Vapour			
Theoretical [cm^{-1}]	Experimental [cm^{-1}]	$\Delta\bar{\nu}$ [cm^{-1}]	% Error
1416.08	1417.50	1.420	0.100
1601.20	1602.88	1.675	0.105
1792.65	1792.75	0.100	0.006
1799.61	1801.38	1.765	0.098
1802.47	1803.13	0.655	0.036
1807.70	1806.88	-0.825	-0.046
1810.62	1809.50	-1.120	-0.062
2018.32	2018.75	0.430	0.021
2041.30	2043.38	2.075	0.102

Table 7

B Task 2

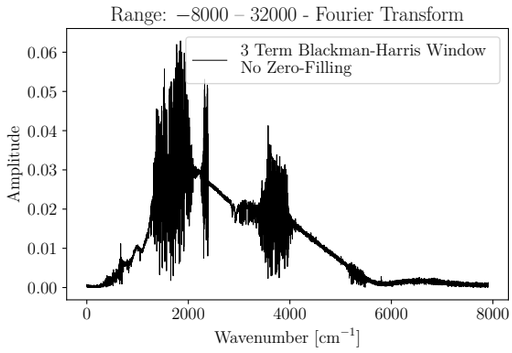

(a) Maximum Mirror Range, no Zerofilling, Blackman-Harris Apodization.

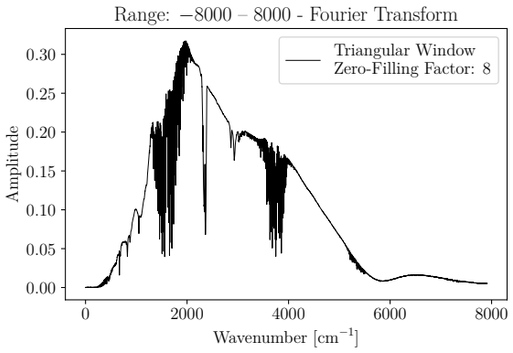

(b) Lower Mirror Range, Zerofilling factor of 8, no Apodization.

Figure 22: Comparison of the two full spectra

Bibliography

[1] Víctor Lórenz-Fonfría and Esteve Padrós. The role and selection of the filter function in fourier self-deconvolution revisited. *Applied spectroscopy*, 63:791–9, 08 2009. doi:10.1366/000370209788701161.

[2] R Nave. Quantum harmonic oscillator. URL: http://hyperphysics.phy-astr.gsu.edu/hbase/quantum/hosc.html.

[3] R Nave. Rotational spectra of rigid rotor molecules. URL: http://hyperphysics.phy-astr.gsu.edu/hbase/molecule/rotrig.html#c3.

[4] Volker Riede and Christian Kranert. Rotation-vibration spectra of molecules experiment for the advanced physics laboratory course. URL: http://www.uni-leipzig.de/%7Ephysfp/manuals/RotVib_englisch.pdf.